Chemical Science

ROYAL SOCIETY OF CHEMISTRY

EDGE ARTICLE

View Article Online
View Journal | View Issue

Cite this: *Chem. Sci.*, 2025, **16**, 21068

All publication charges for this article have been paid for by the Royal Society of Chemistry

Over 260-fold enhancement of reverse intersystem crossing by a host–guest exciplex for a multiple resonance emitter toward efficient narrowband electroluminescence

Zetian Wang, Ting Li, Yongjun Song, Dajun Zhuang, Sen Yang and Lei He *

Multiple resonance (MR) thermally activated delayed fluorescence (TADF) emitters hold great potential for fabricating high-efficiency narrowband organic light-emitting diodes (OLEDs) toward high-definition display applications. However, their slow reverse intersystem crossing (RISC) causes strong device efficiency roll-offs. Reported strategies to enhance the RISC rates (k_{RISC}) of MR-TADF emitters are based on chemical modification of the emitters, which complicates molecular design and synthesis and easily causes widened emission spectra. Here, by utilizing a delicately designed host–guest exciplex, the k_{RISC} of a MR-TADF emitter is significantly enhanced without sacrificing the narrow emission bandwidth. By closely aligning the energy levels of the host and MR-TADF guest, the host–guest ^{3}exciplex state is efficiently formed, which serves as an intermediate triplet state to largely accelerate the RISC of the guest. By embedding a S/Se heavy atom into the host, the heavy atom is directly involved in the ^{3}exciplex state, which markedly strengthens the spin–orbital coupling and boosts the RISC. With the above strategy, host materials for a typical MR-TADF emitter (DtBuCzB) are designed and synthesized. The formed host–guest exciplex significantly boosts the k_{RISC} of DtBuCzB by over 260-fold to 2.2×10^6 s^{-1}, while the emission color and narrow emission bandwidth are both preserved. Narrowband OLEDs using the hosts and DtBuCzB guest show maximum external quantum efficiencies (EQEs) up to 28.7% and EQEs at 1000 cd m^{-2} (EQE_{1000}) up to 23.3%, with the EQE_{1000} values being the highest among non-sensitized narrowband OLEDs based on DtBuCzB reported so far.

Received 6th August 2025
Accepted 6th October 2025

DOI: 10.1039/d5sc05928c

rsc.li/chemical-science

Introduction

Multiple resonance (MR) emitters have aroused tremendous research interest for the fabrication of narrowband organic light-emitting diodes (OLEDs) for high-definition display applications.[1–4] MR emitters usually feature polycyclic aromatic hydrocarbon frameworks embedded with electron-rich and electron-deficient atoms/groups.[1–4] The highest occupied molecular orbital (HOMO) and the lowest unoccupied molecular orbital (LUMO) of MR emitters exhibit alternate distributions on single atoms, which narrows the emission spectrum and meanwhile reduces the energy gap (ΔE_{ST}) between the lowest lying singlet (S_1) and triplet (T_1) states.[1] The reduced ΔE_{ST} triggers reverse intersystem crossing (RISC) and thermally activated delayed fluorescence (TADF),[1,5] which enables utilization of both singlet and triplet excitons in OLEDs, leading to highly efficient narrowband emissive devices.[2–4]

MR-TADF emitters, such as archetypal *ν*-DABNA and DtBuCzB (Fig. 1), usually show low RISC rates (k_{RISC}) (10^3–10^4 s^{-1}), which cause strong accumulation of triplet excitons in OLEDs and severe device efficiency roll-offs.[1,6,7] Sensitized narrowband OLEDs are fabricated by adding sensitizers into the emissive layers to reduce the efficiency roll-offs,[8,9] which however require ternary co-evaporation, complicating the device fabrication. Tremendous efforts have thus been devoted to directly accelerating the RISC of MR-TADF emitters by either reducing the ΔE_{ST} or strengthening the spin–orbital coupling (SOC) between the singlet and triplet states, as illustrated in Fig. 1.[10,11] Extension of the MR framework reduces the ΔE_{ST} (Fig. 1a),[10–25] while integration of heavy atoms (such as S, Se or heavy metal atoms) into the emitters strengthens the SOC (Fig. 1b).[10,11,26–40] Peripheral decoration of MR-TADF emitters with donor/acceptor groups can reduce the ΔE_{ST} or introduce higher-lying long-range charge-transfer triplet states (^{3}LRCT) into the emitters (Fig. 1c).[10,11,41–56] Importantly, the introduced ^{3}LRCT state largely accelerates the RISC of the MR-TADF core by serving as a critical intermediate triplet state, due to the rational SOC between the ^{3}LRCT state and the short-range charge-transfer singlet state (^{1}SRCT) of the MR-TADF core.[44–56] So far,

Key Laboratory of Pesticide and Chemical Biology of Ministry of Education, Hubei International Scientific and Technological Cooperation Base of Pesticide and Green Synthesis, College of Chemistry, Central China Normal University, Wuhan 430079, People's Republic of China. E-mail: helei@ccnu.edu.cn

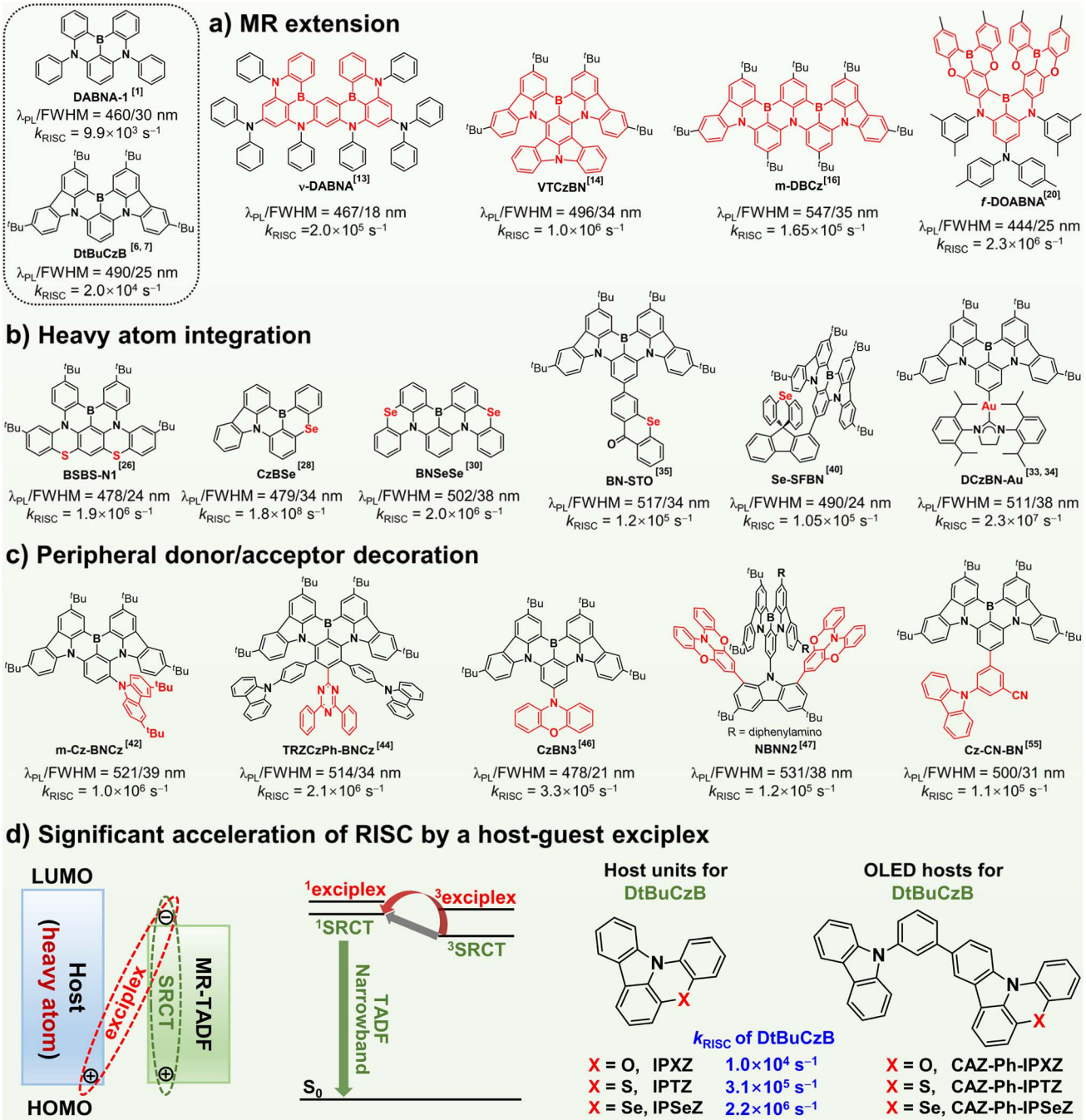

Fig. 1 Strategies to significantly enhance the k_{RISC} values of MR-TADF emitters: (a) MR extension, (b) heavy atom integration, (c) peripheral donor/acceptor decoration, and (d) acceleration of RISC by a host–guest exciplex. Peak emission wavelength (λ_{PL}) and FWHM of the emitters doped in films were quoted, except for VTCzBN, BNSeSe, Se-SFBN, TRZCzPh-BNCz and CzBN3, the λ_{PL} and FWHM of which were recorded in toluene solution.

reported strategies to significantly enhance the k_{RISC} values of MR-TADF emitters have been focused on molecular engineering of the emitters, which complicates molecular design and synthesis and easily causes red-shifted emission with widened emission spectra (Fig. 1a–c).[10,11] Significantly accelerating the RISC of MR-TADF emitters with a facile, efficient strategy while maintaining the narrowband emission has remained a formidable challenge.

The ^{3}exciplex state formed between a host and a MR-TADF guest has intrinsic ^{3}LRCT nature, which could potentially accelerate the RISC of the MR-TADF guest by serving as an intermediate triplet state. This external perturbation strategy does not require molecular engineering of the MR-TADF emitter and could preserve the narrowband emission. Utilizing a host–guest ^{3}exciplex as an intermediate triplet state promises to be a facile, efficient strategy to largely boost the k_{RISC} of a MR-TADF

emitter. However, significantly boosting the k_{RISC} of a MR-TADF emitter to the high level of 10^5–10^6 s^{-1} by a host–guest exciplex has so far not been demonstrated, let alone reducing the device efficiency roll-offs by a host–guest exciplex. Here, using a delicately designed host–guest exciplex, the k_{RISC} of a typical MR-TADF emitter is significantly boosted to 10^5–10^6 s^{-1}, which translates into markedly suppressed device efficiency roll-offs. As illustrated in Fig. 1d, by closely aligning the HOMO levels of the host and MR-TADF guest, the host–guest ^{1}exciplex/^{3}exciplex states are efficiently formed, with the ^{3}exciplex state acting effectively as an intermediate triplet state to accelerate the RISC of the MR-TADF guest.[47,57] Moreover, by embedding a heavy atom into the host, the heavy atom is directly involved in the ^{3}exciplex state, which largely strengthens the SOC between the ^{3}exciplex and ^{1}SRCT states and thus remarkably boosts the RISC. With this strategy, three donor-type host units, IPXZ, IPTZ and IPSeZ (Fig. 1d), are designed and synthesized, the HOMO levels of which approach that of a typical MR-TADF emitter, DtBuCzB. S and Se heavy atoms are embedded into IPTZ and IPSeZ, respectively. Notably, the exciplex formed between IPSeZ and DtBuCzB boosts the k_{RISC} of DtBuCzB by over 260-fold to 2.2 $\times$ 10^6 s^{-1}, while the emission color and narrow emission bandwidth are both preserved. Theoretical calculations and experimental work both show that the external heavy atom effect of the host plays a minor role, while the host–guest exciplex plays a key role, in significant acceleration of the RISC. Three host materials, CAZ-Ph-IPXZ, CAZ-Ph-IPTZ and CAZ-Ph-IPSeZ (Fig. 1d), are designed and synthesized by incorporating the host units. Narrowband OLEDs using the hosts and DtBuCzB guest show maximum external quantum efficiencies (EQEs) up to 28.7% and EQEs at 1000 cd m^{-2} (EQE_{1000}) up to 23.3%, with the EQE_{1000} values being the highest among non-sensitized narrowband OLEDs based on DtBuCzB (reported EQE_{1000} < 15.7%) (Table S1).

Results and discussion

Theoretical calculations

Theoretical calculations were conducted for the [host unit: DtBuCzB] combinations with density functional theory (DFT) at the M062X/6-31G* level. Fig. S1 shows the optimized geometries for the [host unit: DtBuCzB] combinations with a face-to-face configuration and surface distributions of frontier molecular orbitals. The host unit can pack parallelly and closely to DtBuCzB, because of the electron-rich and partially electron-deficient character of the host unit and DtBuCzB, respectively.[58] For the optimized [host unit: DtBuCzB], the LUMO is delocalized over DtBuCzB, whereas the HOMO and HOMO-1 are delocalized over the host unit and DtBuCzB, respectively (Fig. S1). The HOMO-1 and LUMO show alternate distributions on single atoms over DtBuCzB, in agreement with the MR nature of DtBuCzB.[6,7] The HOMO and HOMO-1 show small energy differences (within 0.2 eV), which suggests that electron transfer within DtBuCzB (HOMO-1 → LUMO) and that from the host unit to DtBuCzB (HOMO → LUMO) could both occur in the excited state, with the former and latter corresponding to the formation of SRCT and exciplex states, respectively.

Time-dependent DFT calculations were further conducted on the optimized [host unit: DtBuCzB] at the M062X/6-31G* level. Table S2 summarizes the characteristics of the S_1 and T_1 states. Natural transition orbital (NTO) analysis was performed to analyze the character of excited states. Fig. 2a shows the NTO analysis for the S_1, S_2, T_1 and T_2 states and that for the T_3 and T_4 states is presented in Fig. S2. Fig. 2b depicts the character and energy levels of low-lying singlet and triplet states as well as the SOC matrix elements (SOCMEs) between the S_1 and low-lying triplet states. For the [host unit: DtBuCzB] combinations, the S_1 states are assigned as the ^{1}SRCT states formed within DtBuCzB, whereas the S_2 states are assigned as the ^{1}exciplex states formed between the host units and DtBuCzB, which are located energetically above the S_1 states by 0.10–0.14 eV (Fig. 2b). The T_1 states are assigned as the ^{3}SRCT states. The T_2 states are a mixture of ^{3}exciplex state and localized $^3\pi$–π^* (^{3}LE) state of the host unit or DtBuCzB. The T_3 and T_4 states are the ^{3}LE states of the host unit or DtBuCzB or a mixture of them. As shown in Fig. 2b, the low-lying triplet states in a single DtBuCzB include one ^{3}SRCT state (T_1) and two ^{3}LE states (T_2 and T_3), which correspond to the ^{3}SRCT state (T_1) and the ^{3}LE states (T_3 and T_4) in [host unit: DtBuCzB], respectively. The T_2 state (^{3}exciplex) in [host unit: DtBuCzB] thus stands out as a unique intermediate triplet state between the ^{1}SRCT and ^{3}SRCT states to accelerate the RISC.

For [IPXZ: DtBuCzB], the S_1 and T_1 states show the same SRCT character and the SOCME between them ($SOCME_{S_1\text{-}T_1}$) (0.06 cm^{-1}) is small, whereas the S_1 and T_2 states show different electronic character and the SOCME between them ($SOCME_{S_1\text{-}T_2}$) increases to 0.16 cm^{-1}, which obeys El-Sayed's rule.[59] For [IPTZ: DtBuCzB] and [IPSeZ: DtBuCzB], the $SOCME_{S_1\text{-}T_1}$ values increase to 0.09 and 0.63 cm^{-1}, respectively, as compared to that (0.06 cm^{-1}) of [IPXZ: DtBuCzB]. Such an increase of $SOCME_{S_1\text{-}T_1}$ is ascribed to the external heavy atom effect of the host, which works by through-space heavy atom–emitter interactions and requires no direct involvement of the heavy atom in related excited-states.[40,60,61] For [IPTZ: DtBuCzB] and [IPSeZ: DtBuCzB], the $SOCME_{S_1\text{-}T_1}$ values largely increase to 0.44 and 3.78 cm^{-1}, respectively, as compared to that (0.16 cm^{-1}) of [IPXZ: DtBuCzB]. On one hand, the SOC between the S_1 and T_2 states with different electronic character is permitted.[59] On the other hand, the S/Se heavy atoms embedded in the host units are directly involved in the T_2 states (^{3}exciplex), which markedly contribute to the SOC between the S_1 and T_2 states. As shown in Fig. 2b, the T_2 states in [host unit: DtBuCzB], with rational SOC with the S_1 states, serve as important intermediate triplet states to accelerate the RISC of DtBuCZB.[44–47] In particular, the T_2 states in [IPTZ: DtBuCzB] and [IPSeZ: DtBuCzB], with considerable SOC with the S_1 states, would act efficiently as intermediate triplet states to largely accelerate the RISC.

Synthesis of the hosts and energy-level alignments

Scheme S1 shows the synthetic routes to IPXZ, IPTZ and IPSeZ. 10*H*-phenoxazine reacted with 1-bromo-2-iodobenzene *via* a copper catalyzed C–N coupling reaction to yield 10-(2-bromophenyl)-10*H*-phenoxazine, which was then converted to

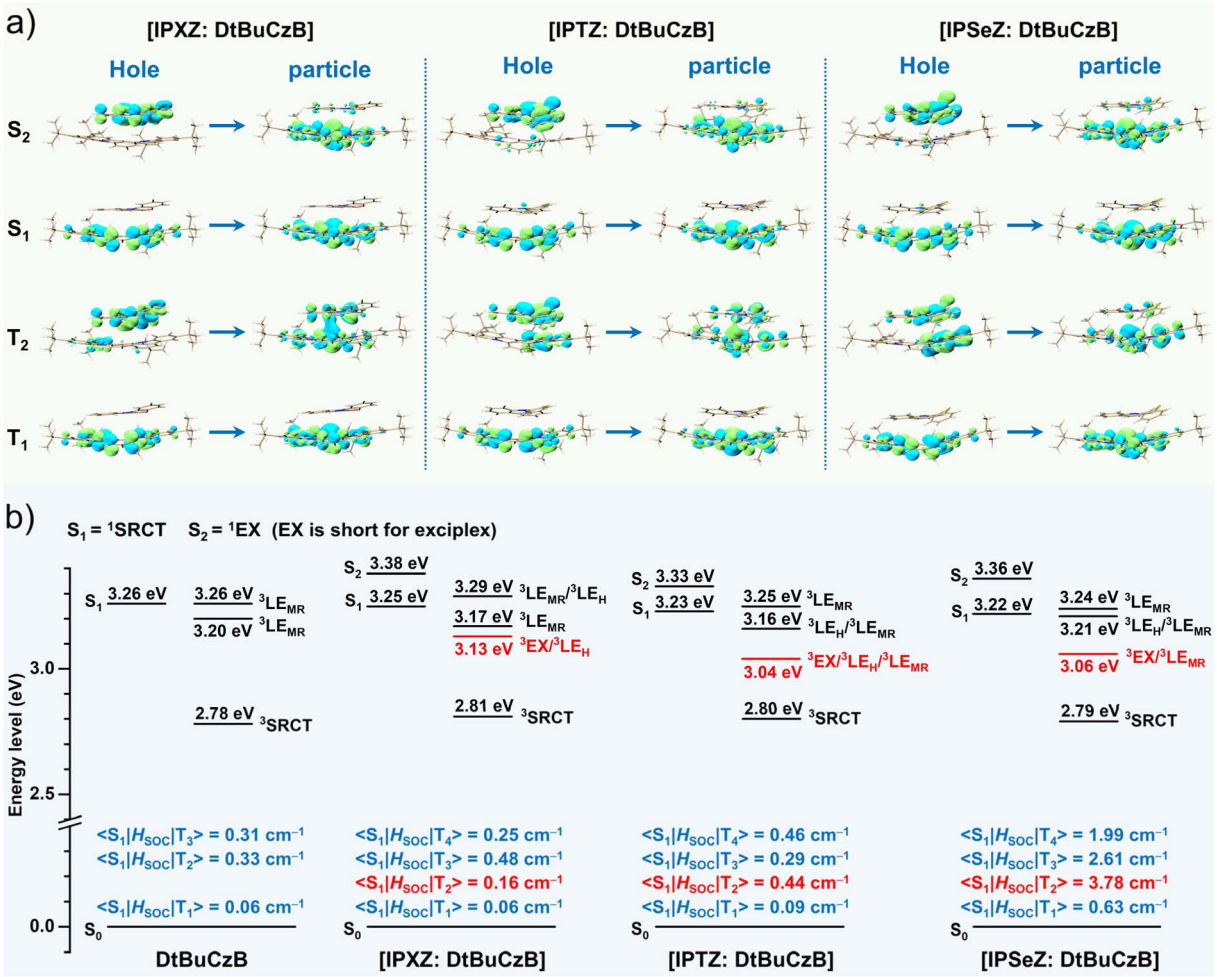

Fig. 2 (a) NTO analysis for the S_1, S_2, T_1 and T_2 states of the [host unit: DtBuCzB] combination. (b) Excited-state energy levels and SOCMEs between the S_1 and low-lying triplet states.

IPXZ by a Pd(II)-catalyzed intramolecular cyclization reaction.[62] IPTZ and IPSeZ were synthesized in a similar way by replacing 10*H*-phenoxazine with 10*H*-phenothiazine and 10*H*-phenoselenazine, respectively. Fig. S3 shows the single-crystal structures of the host units. IPXZ shows an almost planar geometry with small torsion angles between two adjacent phenyl rings at 1.5° and 2.2°. IPTZ and IPSeZ show less planar geometries with larger torsion angles (5.7–8.8° and 24.0–25.2°) between two adjacent phenyl rings, because the large-size sulfur and selenium atoms distort the molecular structures.

Cyclic voltammetry measurements were performed for the host units in solution. Fig. S4a shows the cyclic voltammograms and Table S3 summarizes the onset oxidation potentials and calculated energy levels. From the onset oxidation potentials, the HOMO levels of IPXZ, IPTZ and IPSeZ were determined at −5.24, −5.25 and −5.32 eV, respectively. Ultraviolet photoelectron spectroscopy measurements were further conducted for the host units in film states (Fig. S5). The obtained ionization potentials agree with the HOMO levels derived from the onset oxidation potentials. Based on the HOMO levels and the optical bandgaps derived from the onsets of absorption spectra (Fig. S6a), the LUMO levels of IPXZ, IPTZ and IPSeZ were determined at −2.03, −2.12 and −2.17 eV, respectively. The HOMO and LUMO levels of selected MR-TADF guests (including DtBuCzB,[6,7] CzB[63] and BN2 [64]) were determined in a similar way (Fig. S4b, S6b and Table S3). Fig. 3 illustrates the energy level alignments between the host units and MR-TADF guests. The HOMO levels of the host units are only slightly lower (by 0.05–0.13 eV) than that of DtBuCzB, whereas the LUMO levels are much higher (by 0.49–0.63 eV) than that of DtBuCzB. Such an energy-level alignment allows facile electron transfer from the HOMO of the host unit to the LUMO of DtBuCzB, giving rise to an exciplex state. In contrast, for the common host mCBP,[57] the HOMO and LUMO levels are considerably lower (by 0.81 eV) and higher (by 0.26 eV), respectively, than the HOMO and LUMO levels of DtBuCzB, which does not support efficient formation of the exciplex (Fig. 3). According to the emission peaks of low-temperature fluorescence and phosphorescence spectra (Fig. S7), the singlet/triplet energies of IPXZ, IPTZ and IPSeZ were determined at 3.28/2.85, 3.11/2.67 and 3.11/2.73 eV, respectively, which are considerably higher than those (2.59/2.46 eV) of DtBuCzB (Table S3).

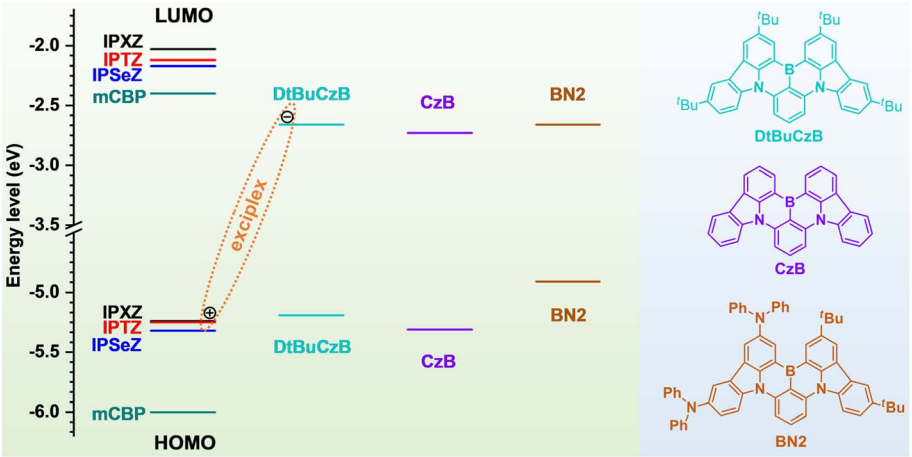

Fig. 3 Energy-level alignments between the host units and MR-TADF guests.

The host materials used for OLEDs, CAZ-Ph-IPXZ, CAZ-Ph-IPTZ and CAZ-Ph-IPSeZ, were prepared with IPXZ, IPTZ and IPSeZ as subunits, respectively. Scheme S2 shows the synthetic routes to the host materials. A single crystal of CAZ-Ph-IPXZ was successfully obtained during temperature-gradient sublimation under high vacuum. Fig. S8 shows the single-crystal structure of CAZ-Ph-IPXZ. Both IPXZ and carbazole units in CAZ-Ph-IPXZ are twisted with respect to the central phenyl linker with torsion angles at 41° and 55°, respectively. Fig. S9 and S10 show the cyclic voltammograms, absorption spectra and fluorescence/phosphorescence spectra of the host materials in solution, from which the HOMO/LUMO levels and singlet/triplet energies of the host materials were determined and are summarized in Table S4. The host materials show similar energy levels and excited-state energies to the corresponding host units (Tables S3 and S4).

Photophysical characterization

Host–guest films with a composition of 30 wt% polystyrene (PS): 69 wt% host unit and 1 wt% DtBuCzB were fabricated by spin-

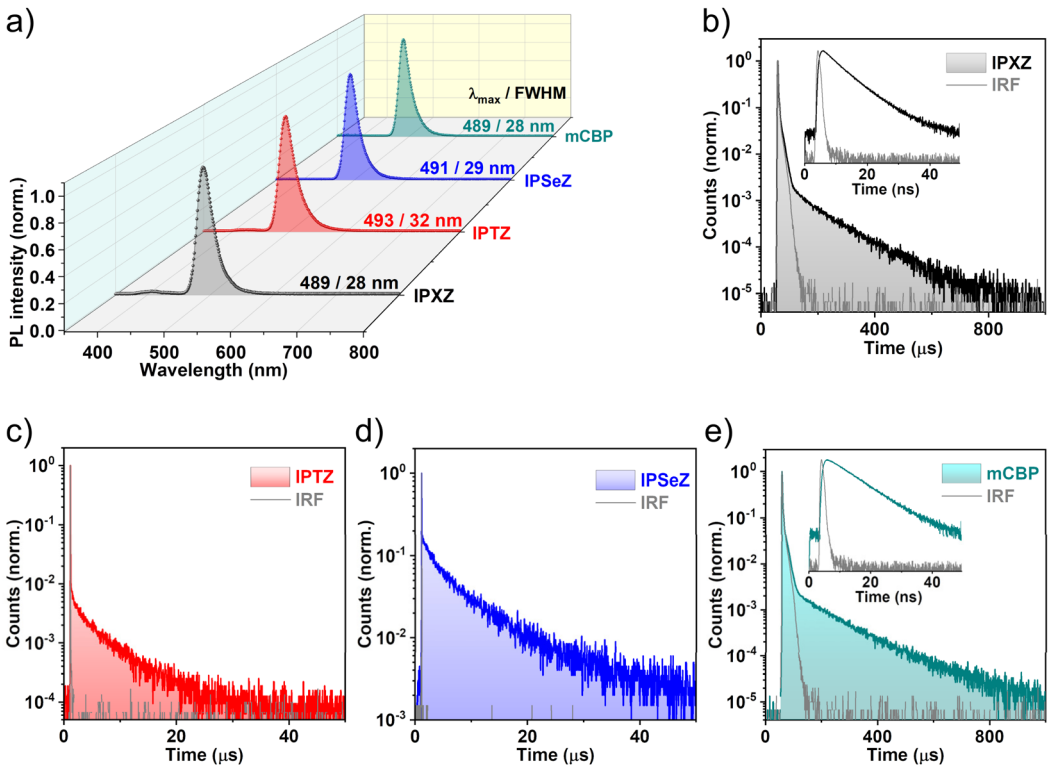

Fig. 4 (a) PL spectra and (b–e) transient PL decay curves of the [PS: host: DtBuCzB] films. The host is IPXZ, IPTZ, IPSeZ or mCBP. The weight ratio between PS, host and DtBuCzB is 30 : 69 : 1. The excitation wavelength is 300 nm.

Table 1 Emission characteristics of the [PS: 69 wt% host: 1 wt% DtBuCzB] films

Host	PL/FWHM [nm]	$\Phi/\Phi_p/\Phi_d$[a]	τ_p [ns]	τ_d [μs]	$E_S/E_T/\Delta E_{ST}$ [eV]	$k_{r,s}$ [b] [10^8 s^{-1}]	k_{ISC} [c] [10^7 s^{-1}]	k_{RISC} [10^4 s^{-1}]
IPXZ	489/28	0.88/0.83/0.05	5.9	110	2.61/2.50/0.11	1.4	0.96	0.96
IPTZ	493/32	0.90/0.59/0.31	5.0	4.9	2.60/2.49/0.11	1.2	6.9	31
IPSeZ	491/29	0.92/0.06/0.86	2.4	7.1	2.59/2.48/0.11	0.25	39	220
mCBP	489/28	0.93/0.86/0.07	8.0	130	2.59/2.46/0.13	1.1	0.94	0.83

[a] Φ_p and Φ_d: prompt and delayed components of photoluminescence efficiency. [b] Radiative decay rate of the singlet state. [c] Intersystem crossing rate.

coating from 1,2-dichloroethane solution. The PS polymer was mixed into the film to increase the film quality. The mCBP host was also used to fabricate a reference host–guest film. Fig. 4a shows the photoluminescence (PL) spectra of the host–guest films. Table 1 summarizes the emission characteristics of the films. The films with IPXZ, IPTZ, IPSeZ and mCBP hosts all show narrowband blue–green emission originating from DtBuCzB, with emission peaks/full widths at half maximum (FWHMs) at 489/28, 493/32, 491/29 and 489/28 nm, respectively. The retained emission color and narrow emission bandwidth indicate that the ^{1}exciplex state formed between the host and DtBuCzB is located energetically above the ^{1}SRCT state of DtBuCzB, as indicated by theoretical calculations (Fig. 2b), and contributes negligibly to the emission.[47]

Fig. 4b–e show the transient PL decay curves of the [PS: host: DtBuCzB] films. The transient decay data are summarized in Table 1. The film with the mCBP host shows a long delayed fluorescence lifetime (τ_d) at 130 μs. The film with the IPXZ host shows a shortened τ_d at 110 μs. Notably, the films with the IPTZ and IPSeZ hosts show significantly shortened τ_d values at 4.9 and 7.1 μs, respectively. No other long delayed components have been observed in the transient PL decay curves for the films with the IPTZ and IPSeZ hosts (Fig. S11). The delayed fluorescence almost disappears upon cooling the films to 77 K (Fig. S12), which agrees with the TADF nature of the emission.[5] The host–guest films all show high photoluminescence quantum efficiencies (Φ_{PL}) at 0.88–0.93. Rate constants of the TADF emission were calculated from the Φ_{PL} and transient PL decay data and are summarized in Table 1. The film with the mCBP host shows a low k_{RISC} value at 8.3×10^3 s^{-1}, whereas the film with the IPXZ host shows an enhanced k_{RISC} value at 9.6×10^3 s^{-1}. Notably, the films with the IPTZ and IPSeZ hosts show over 30-fold and 260-fold higher k_{RISC} values at 3.1×10^5 and 2.2×10^6 s^{-1}, respectively. The [PS: IPSeZ: DtBuCzB] film exhibits a much higher k_{RISC} than the [PS: IPTZ: DtBuCzB] film, although the two films have similar τ_d values. This is because the [PS: IPSeZ: DtBuCzB] film has much stronger delayed fluorescence, as shown by its much larger delayed component of photoluminescence efficiency (Table 1). The ΔE_{ST} values of the [PS: host: DtBuCzB] films were determined from the low-temperature fluorescence and phosphorescence spectra (Fig. S13), which fall between 0.11 and 0.13 eV and are close to the ΔE_{ST} (0.13 eV) reported for DtBuCzB.[6] The similar ΔE_{ST} values indicate that the significant acceleration of RISC is unlikely to be caused by reduction of ΔE_{ST}. As shown by theoretical calculations, the ^{3}exciplex states (T_2 states) in [IPTZ: DtBuCzB] and [IPSeZ: DtBuCzB] show considerable SOC with the ^{1}SRCT state (S_1) of DtBuCzB and thereby can act efficiently as intermediate triplet states to significantly accelerate the RISC of DtBuCzB, which is experimentally verified here. Theoretical calculations also reveal that the energy gap (0.32 eV) between the ^{3}exciplex (T_2) and ^{3}SRCT (T_1) states in [IPXZ: DtBuCzB] is larger than those (0.24 and 0.27 eV) in [IPTZ: DtBuCzB] and [IPSeZ: DtBuCzB] (Fig. 2b). Moreover, the ^{3}exciplex (T_2) and ^{1}SRCT (T_1) states in [IPXZ: DtBuCzB] exhibit a smaller SOCME than those in [IPTZ: DtBuCzB] and [IPSeZ: DtBuCzB], due to the lack of heavy atoms in IPXZ. These theoretical calculation results suggest that the ^{3}exciplex state in [IPXZ: DtBuCzB] acts less efficiently as an intermediate triplet state to accelerate the RISC of DtBuCzB, which explains the lower k_{RISC} of the [PS: IPXZ: DtBuCzB] film. However, the k_{RISC} (9.6×10^3 s^{-1}) of the [PS: IPXZ: DtBuCzB] film is still larger than that (8.3×10^3 s^{-1}) of the [PS: mCBP: DtBuCzB] film. In the latter film, efficient formation of the host–guest exciplex is not supported.

The energy level of an exciplex state formed between a donor and an acceptor is expressed by

$$E_{exciplex} = \Delta E + C = E_{LUMO,A} - E_{HOMO,D} + C \quad (1)$$

where ΔE is the energy gap between the LUMO of the acceptor (here the MR-TADF guest) and the HOMO of the donor (here the host unit) and C is a constant related to the coulombic potential energy within the electron–hole pair of the exciplex.[65] It should be noted that the ^{1}exciplex and ^{3}exciplex states have nearly identical energy levels, because of the tiny spin-exchange energy between them.[66] As shown in Fig. 3, the MR-TADF guest CzB has a lower (by 0.08 eV) LUMO level than DtBuCzB, which suggests that the energy level of the exciplex state formed in [host unit: CzB] would be lowered compared to that formed in [host unit: DtBuCzB], according to eqn (1). CzB also shows blue-shifted emission and has higher (by 0.03–0.05 eV) energy levels of ^{1}SRCT/^{3}SRCT states as compared to DtBuCzB (Table S3).[63] It is thus expected that the energy gap between the ^{1}exciplex (^{3}exciplex) and ^{1}SRCT (^{3}SRCT) states in [host unit: CzB] would be reduced compared to that in [host unit: DtBuCzB], as illustrated in Fig. S14. Fig. S15a shows the PL spectra of the [PS: host: CzB] films. Table S5 summarizes the emission characteristics of the films. The films with the IPXZ, IPTZ, IPSeZ and mCBP hosts show emission peaks/FWHMs at 480/32, 490/71, 490/49 and 481/31 nm, respectively. The films with the IPXZ and mCBP

hosts still show narrowband emission, whereas the films with the IPTZ and IPSeZ hosts show red-shifted emission with largely widened emission spectra, which reflects the emergence of exciplex emission, due to the reduced energy gap between the ^{1}exciplex and ^{1}SRCT states (Fig. S14).[47] The gradual red-shift and broadening of the emission spectrum upon changing the host unit from IPXZ, to IPSeZ, and to IPTZ suggests that the contribution to the emission by the exciplex state increases in that order. Because an exciplex state located energetically closer to the ^{1}SRCT state is more likely to contribute to the emission, it also suggests that the energy level of the exciplex state decreases upon changing the host unit from IPXZ, to IPSeZ, and to IPTZ in [host unit: CzB]. In other words, the tendency to form the exciplex increases upon changing the host unit from IPXZ, to IPSeZ and to IPTZ. For the [PS: host: DtBuCzB] films, the emission spectrum is slightly red-shifted and broadened upon changing the host unit from IPXZ, to IPSeZ, and to IPTZ (Fig. 4a), which agrees with the energy-level order of the exciplex state.

Fig. S15b and 15c show the transient PL decay curves of the [PS: host: CzB] films. Table S5 summarizes the transient decay data and calculated rate constants of the TADF emission. The [PS: mCBP: CzB] film shows a long τ_d at 78 μs and a low k_{RISC} at 1.5×10^4 s^{-1}, whereas the [PS: IPXZ: CzB] film shows a shortened τ_d at 45 μs and a considerably higher k_{RISC} at 2.5×10^4 s^{-1}. For comparison, the [PS: IPXZ: DtBuCzB] film only shows a slightly higher k_{RISC} (9.6×10^3 s^{-1}) than the [PS: mCBP: DtBuCzB] film (8.3×10^3 s^{-1}). It is thus suggested that the ^{3}exciplex state in [IPXZ: CzB] acts more efficiently as an intermediate triplet state to accelerate the RISC of the MR-TADF guest as compared to the ^{3}exciplex state in [IPXZ: DtBuCzB], due to the reduced energy gap between the ^{3}exciplex and ^{3}SRCT states in [IPXZ: CzB] (Fig. S14). It is shown here that an ^{3}exciplex state located energetically close to the ^{3}SRCT state can act as an intermediate triplet state to accelerate the RISC of the MR-TADF guest, which agrees with a previous report that an intramolecular through-space charge-transfer state accelerates the RISC of a MR-TADF unit.[47]

BN2 was further used as a MR-TADF guest to fabricate host–guest films. As shown in Fig. 3, BN2 has a considerably shallower (by 0.29–0.37 eV) HOMO level than the host units, which suggests that the exciplex formation between the host unit and BN2 is much less efficient. BN2 shows an almost identical LUMO level to DtBuCzB, which suggests that the ^{1}exciplex/^{3}exciplex states formed in [host unit: BN2] would have similar energy levels to those formed in [host unit: DtBuCzB], according to eqn (1). However, BN2 shows largely red-shifted emission and has considerably lower (by 0.13–0.17 eV) energy levels of ^{1}SRCT/^{3}SRCT states compared to DtBuCzB (Table S3).[64] It is thus expected that the energy gap between the ^{1}exciplex (^{3}exciplex) and ^{1}SRCT (^{3}SRCT) states in [host unit: BN2] would be largely enlarged compared to that in [host unit: DtBuCzB], as illustrated in Fig. S14. Fig. S16 shows the PL spectra and transient PL decay curves of the [PS: host: BN2] films. Table S6 summarizes the emission characteristics of the films. The films all show narrowband green–yellow emission (Fig. S16a), which indicates that the ^{1}exciplex state makes nearly no contribution to the emission, due to the large energy gap between the ^{1}exciplex and ^{1}SRCT states (Fig. S14). The films with IPXZ, IPTZ, IPSeZ and mCBP hosts show long τ_d values at 550, 780, 510, and 590 μs, respectively, and low k_{RISC} values at 2.0×10^3, 2.1×10^3, 4.9×10^3 and 1.9×10^3 s^{-1}, respectively. The [PS: IPSeZ: BN2] film only shows a 1.5-fold higher k_{RISC} than the [PS: mCBP: BN2] film. In the [PS: host: BN2] films, the ^{3}exciplex states would act much less efficiently as intermediate triplet states to accelerate the RISC, due to the largely increased energy gap between the ^{3}exciplex and ^{3}SRCT states (Fig. S14). The 1.5-fold increase of k_{RISC} for the [PS: IPSeZ: BN2] film should result from the external heavy atom effect of the IPSeZ host, which works by through-space heavy atom–emitter interactions.[40,60,61] Previous reports have shown that the external heavy atom effect of the host increases the k_{RSIC} of the TADF guest by several fold.[40,60,61] Here, it is shown that the external heavy atom effect of the host is capable of accelerating the RISC of the MR-TADF guest by several fold, but it is unable to significantly accelerate the RISC by orders of magnitude. When an ^{3}exciplex state is located energetically close to the ^{3}SRCT state and involves a heavy atom of the host, the RISC of the MR-TADF guest is significantly accelerated by orders of magnitude, as observed for the [PS: IPTZ: DtBuCzB] and [PS: IPSeZ: DtBuCzB] films. These results highlight the great importance of forming a host–guest exciplex in maximizing the heavy atom effect of the host to significantly accelerate the RISC of the TADF guest.

To gain further evidence on the exciplex formation between the host unit and MR-TADF guest, time-resolved PL spectra were measured for the host–guest films. Fig. S17a–d show the time-resolved PL spectra of the [PS: host: DtBuCzB] films with mCBP, IPXZ, IPTZ and IPSeZ as the hosts, respectively. As mentioned above, the [PS: mCBP: DtBuCzB], [PS: IPXZ: DtBuCzB] and [PS: IPSeZ: DtBuCzB] films exhibit nearly no exciplex emission, as indicated by their maintained narrow emission spectra (Fig. 4a and Table 1), because the ^{1}exciplex states are located higher in energy than the ^{1}SRCT states. Accordingly, the emission spectra of these films show negligible changes and maintained narrow bandwidths with time evolution after excitation (Fig. S17a, b and d). In contrast, the [PS: IPTZ: DtBuCzB] film exhibits some exciplex emission, as indicated by its slightly red-shifted and widened emission spectrum (Fig. 4a and Table 1), because the ^{1}exciplex state gets closer in energy to the ^{1}SRCT state. The emission spectrum of the [PS: IPTZ: DtBuCzB] film is gradually broadened with time evolution after excitation (Fig. S17c), which involves the formation of an exciplex between IPTZ and DtBuCzB in excited states and subsequent emission from the ^{1}exciplex state. To further reveal the exciplex formation, time-resolved PL spectra of the [PS: IPTZ: CzB] film have been measured (Fig. S17e). As aforementioned, the [PS: IPTZ: CzB] film exhibits considerable exciplex emission, as indicated by its largely widened emission spectrum (Fig. S15a). Accordingly, the emission spectrum of the [PS: IPTZ: CzB] film is gradually broadened to a large extent with time evolution after excitation (Fig. S17e), in agreement with the formation of the exciplex between IPTZ and CzB in excited states and intensified exciplex emission.

Fig. S18 shows the PL spectra and transient PL decay curves of the host–guest films with the CAZ-Ph-IPXZ, CAZ-Ph-IPTZ or CAZ-Ph-IPSeZ host materials and the DtBuCzB guest. Table S7 summarizes the emission characteristics of the films. Because of the similar energy levels and excited-state energies of the host materials to the host units (Tables S3 and S4), the host–guest films with the host materials show similar emission characteristics to the host–guest films with the host units (Tables 1 and S7). As shown in Fig. S18a, the host–guest films all show narrowband blue–green emission originating from DtBuCzB. As observed for the IPTZ and IPSeZ host units, the CAZ-Ph-IPTZ and CAZ-Ph-IPSeZ host materials largely shorten the τ_d of DtBuCzB to 6.5 and 6.6 μs, respectively, and significantly enhance the k_{RISC} of DtBuCzB to 2.2×10^5 and 2.2×10^6 s^{-1}, respectively. The [PS: CAZ-Ph-IPXZ: DtBuCzB] film shows the τ_d/k_{RISC} at 117 μs/9.5×10^3 s^{-1}, which resemble those (110 μs/9.6×10^3 s^{-1}) of the [PS: IPXZ: DtBuCzB] film.

Narrowband OLEDs

CAZ-Ph-IPXZ, CAZ-Ph-IPTZ and CAZ-Ph-IPSeZ were used as hosts for DtBuCzB to fabricate narrowband OLEDs. Fig. 5a shows the structure and energy-level diagram of the device as well as the chemical structures of the used materials. Fig. 5b shows the electroluminescence (EL) spectra of the OLEDs. The OLEDs based on CAZ-Ph-IPXZ1, CAZ-Ph-IPTZ and CAZ-Ph-IPSeZ all showed narrowband blue–green EL with emission peaks/FWHMs at 490/28, 493/33 and 491/29 nm, respectively. The EL spectra remained almost the same under different driving voltages (Fig. S19). Fig. 5c and d show the current density–voltage–luminance and EQE–luminance curves of the OLEDs. The device performances are summarized in Table 2. The devices based on CAZ-Ph-IPXZ, CAZ-Ph-IPTZ and CAZ-Ph-IPSeZ showed EQE_{max}/EQE_{1000} at 26.5%/13.6%, 28.7%/22.2% and 28.5%/23.3%, respectively, with efficiency roll-offs at 49%, 22% and 18%, respectively. The device with a conventional mCBP host was also fabricated, which showed EQE_{max}/EQE_{1000} at 22.5%/8.9% (Fig. S20 and Table 2), exhibiting a large efficiency roll-off at 60%. Compared to the device based on mCBP, the devices based on CAZ-Ph-IPXZ, CAZ-Ph-IPTZ and CAZ-Ph-IPSeZ showed higher EQE_{1000} and smaller efficiency roll-offs, due to the accelerated RISC of DtBuCzB. In particular, the devices based on CAZ-Ph-IPTZ and CAZ-Ph-IPSeZ showed remarkably higher EQE_{1000} and smaller efficiency roll-offs, due to the

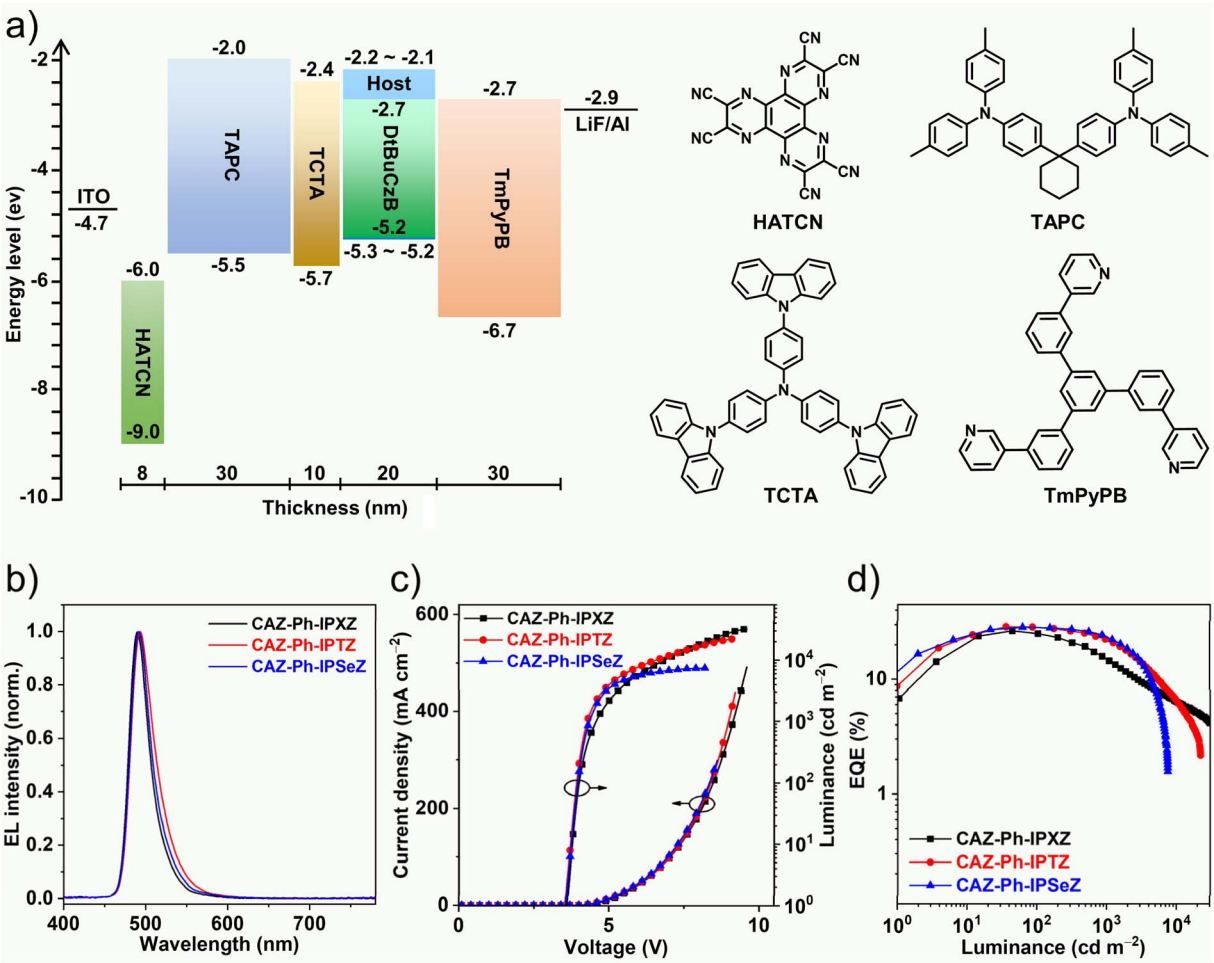

Fig. 5 (a) Device structure, (b) EL spectra, (c) current density–voltage–luminance curves, and (d) EQE–luminance curves of the OLEDs with CAZ-Ph-IPXZ, CAZ-Ph-IPTZ or CAZ-Ph-IPSeZ as the host and DtBuCzB (2.0 wt%) as the guest.

Table 2 Summary of performances of the OLEDs[a]

	V_{on}[b] [V]	η_c[c] [cd A^{-1}]	EQE[d] [%]	EL λ [nm]	FWHM [nm]	CIE [x, y]
CAZ-Ph-IPXZ	3.5	48.1/45.3/24.8	26.5/25.0/13.6	489	28	0.088, 0.410
CAZ-Ph-IPTZ	3.5	63.9/63.0/49.2	28.7/28.3/22.2	493	33	0.105, 0.490
CAZ-Ph-IPSeZ	3.5	57.1/56.3/46.5	28.5/28.2/23.3	491	29	0.097, 0.450
mCBP	3.5	36.7/28.0/14.4	22.5/17.2/8.9	488	28	0.092, 0.353

[a] Doping concentration of DtBuCzB in the emissive layer is 2.0 wt%. [b] Voltage to reach 1 cd m^{-2}. [c] Maximum current efficiency and the values at 100 and 1000 cd m^{-2}. [d] Maximum EQE and the values at 100 and 1000 cd m^{-2}.

significantly accelerated RISC of DtBuCzB. Fig. S21 shows the current density–voltage curves of the single-carrier devices based on CAZ-Ph-IPXZ, CAZ-Ph-IPTZ and CAZ-Ph-IPSeZ hosts. The hole-only devices showed similar hole currents (Fig. S21a), whereas the electron-only devices showed largely differed electron-currents, with the electron-current being largely decreased upon changing the host material from CAZ-Ph-IPXZ, to CAZ-Ph-IPTZ, and to CAZ-Ph-IPSeZ, especially at high driving voltages (Fig. S21b). These results suggest that the electron–hole recombination at high driving voltage becomes much more unbalanced upon changing the host material from CAZ-Ph-IPXZ, to CAZ-Ph-IPTZ, and to CAZ-Ph-IPSeZ. This would explain the rapid decrease of EQE at high luminance (over 1000 cd m^{-2}) for the devices based on CAZ-Ph-IPTZ and CAZ-Ph-IPSeZ (Fig. 5d).

It is noteworthy that the EQE_{1000} values (22.2% and 23.3%) of the devices with the CAZ-Ph-IPTZ and CAZ-Ph-IPSeZ hosts are the highest among non-sensitized narrowband OLEDs based on DtBuCzB reported so far (reported EQE_{1000} < 15.7%) (Table S1). They are also superior/comparable to those (15.9%–27.7%) of sensitized narrowband OLEDs based on DtBuCzB reported so far (Table S1). TADF/phosphorescence sensitizers have been incorporated into MR-TADF OLEDs to effectively suppress the efficiency roll-offs,[8,9,67] which however requires ternary co-evaporation. The significant acceleration of RISC by a host–guest exciplex enables fabrication of high-efficiency MR-TADF OLEDs with suppressed efficiency roll-offs through binary co-evaporation, which simplifies the device fabrication process and would be beneficial for commercial production.

Conclusion

Significant acceleration of the RISC of a typical MR-TADF emitter was achieved by utilizing a delicately designed host–guest exciplex. Donor-type host materials were developed with the HOMO levels approaching that of a typical MR-TADF guest, DtBuCzB. Theoretical calculations and experimental work revealed that the host–guest ^{1}exciplex/^{3}exciplex states were efficiently formed and located above but close to the ^{1}SRCT/^{3}SRCT states of the DtBuCzB guest, enabling the ^{3}exciplex state to act efficiently as an intermediate triplet state to accelerate the RISC of DtBuCzB. The heavy atom embedded in the host was directly involved in the ^{3}exciplex state, which largely strengthened the SOC between the ^{3}exciplex and ^{1}SRCT states and thus remarkably boosted the RISC of DtBuCzB. The host–guest exciplex significantly enhanced the k_{RISC} of DtBuCzB by over 260-fold to 2.2 × 10^6 s^{-1}, while the emission color and narrow emission bandwidth were both preserved. Theoretical calculations and experimental work both showed that the host–guest exciplex, rather than the external heavy atom effect of the host, played a decisive role in markedly boosting the RISC. Non-sensitized narrowband OLEDs using the hosts and DtBuCzB guest showed maximum EQEs up to 28.7% and significantly suppressed efficiency roll-offs, with EQE_{1000} values remaining up to 23.3%. The work demonstrates the huge potential of a host–guest exciplex for significantly accelerating the RISC of MR-TADF guest for the fabrication of high-efficiency narrowband OLEDs with suppressed efficiency roll-offs.

Author contributions

Z. Wang: methodology, investigation, data curation, formal analysis, visualization, and writing – original draft; T. Li: methodology, investigation, and validation; Y. Song: investigation and validation; D. Zhuang: investigation and validation; S. Yang: investigation and validation; L. He: conceptualization, supervision, project administration, methodology, resources, funding acquisition, and writing – review and editing.

Conflicts of interest

The authors declare no conflict of interest.

Data availability

CCDC 2435331, 2435332, 2435333 and 2435337 contain the supplementary crystallographic data for this paper.[68a–d]

The data supporting this article have been included within the article or as part of the supplementary information (SI). Supplementary information: experimental methods, synthetic procedures, NMR and mass spectrometry data of the compounds, crystallographic data, theoretical calculation data, photophysical data and device performance data. See DOI: **https://doi.org/10.1039/d5sc05928c**.

Acknowledgements

We thank the Fundamental Research Funds for the Central Universities (Grant No. CCNU22QN008) and the Program of

Introducing Talents of Discipline to Universities of China (111 Program, B17019) for financial support.

References

1 T. Hatakeyama, K. Shiren, K. Nakajima, S. Nomura, S. Nakatsuka, K. Kinoshita, J. Ni, Y. Ono and T. Ikuta, *Adv. Mater.*, 2016, **28**, 2777–2781.
2 H. J. Kim and T. Yasuda, *Adv. Opt. Mater.*, 2022, **10**, 2201714.
3 H. Jiang, J. Jin and W.-Y. Wong, *Adv. Funct. Mater.*, 2023, **33**, 2306880.
4 M. Mamada, M. Hayakawa, J. Ochi and T. Hatakeyama, *Chem. Soc. Rev.*, 2024, **53**, 1624–1692.
5 H. Uoyama, K. Goushi, K. Shizu, H. Nomura and C. Adachi, *Nature*, 2012, **492**, 234–238.
6 Y. Xu, Z. Cheng, Z. Li, B. Liang, J. Wang, J. Wei, Z. Zhang and Y. Wang, *Adv. Opt. Mater.*, 2020, **8**, 1902142.
7 M. Yang, I. S. Park and T. Yasuda, *J. Am. Chem. Soc.*, 2020, **142**, 19468–19472.
8 Y. Zhang, D. Zhang, J. Wei, X. Hong, Y. Lu, D. Hu, G. Li, Z. Liu, Y. Chen and L. Duan, *Angew. Chem., Int. Ed.*, 2020, **59**, 17499–17503.
9 Y. Zhang, J. Wei, D. Zhang, C. Yin, G. Li, Z. Liu, X. Jia, J. Qiao and L. Duan, *Angew. Chem., Int. Ed.*, 2022, **61**, e202113206.
10 K. R. Naveen, P. Palanisamy, M. Y. Chae and J. H. Kwon, *Chem. Commun.*, 2023, **59**, 3685–3702.
11 X.-F. Luo, X. Xiao and Y.-X. Zheng, *Chem. Commun.*, 2024, **60**, 1089–1099.
12 A. Pershin, D. Hall, V. Lemaur, J.-C. Sancho-Garcia, L. Muccioli, E. Zysman-Colman, D. Beljonne and Y. Olivier, *Nat. Commun.*, 2019, **10**, 597.
13 Y. Kondo, K. Yoshiura, S. Kitera, H. Nishi, S. Oda, H. Gotoh, Y. Sasada, M. Yanai and T. Hatakeyama, *Nat. Photonics*, 2019, **13**, 678–682.
14 X. F. Luo, S. Q. Song, H. X. Ni, H. Ma, D. Yang, D. Ma, Y. X. Zheng and J. L. Zuo, *Angew. Chem., Int. Ed.*, 2022, **61**, e202209984.
15 S. Oda, B. Kawakami, Y. Yamasaki, R. Matsumoto, M. Yoshioka, D. Fukushima, S. Nakatsuka and T. Hatakeyama, *J. Am. Chem. Soc.*, 2022, **144**, 106–112.
16 X. Cai, Y. Pu, C. Li, Z. Wang and Y. Wang, *Angew. Chem., Int. Ed.*, 2023, **62**, e202304104.
17 F. Huang, X.-C. Fan, Y.-C. Cheng, H. Wu, X. Xiong, J. Yu, K. Wang and X.-H. Zhang, *Angew. Chem., Int. Ed.*, 2023, **62**, e202306413.
18 Y. Sano, T. Shintani, M. Hayakawa, S. Oda, M. Kondo, T. Matsushita and T. Hatakeyama, *J. Am. Chem. Soc.*, 2023, **145**, 11504–11511.
19 B. Lei, Z. Huang, S. Li, J. Liu, Z. Bin and J. You, *Angew. Chem., Int. Ed.*, 2023, **62**, e202218405.
20 R. W. Weerasinghe, S. Madayanad Suresh, D. Hall, T. Matulaitis, A. M. Z. Slawin, S. Warriner, Y. T. Lee, C. Y. Chan, Y. Tsuchiya, E. Zysman-Colman and C. Adachi, *Adv. Mater.*, 2024, **36**, 2402289.
21 S. Xiao, X. Cao, G. Chen, X. Yin, Z. Chen, J. Miao and C. Yang, *Angew. Chem., Int. Ed.*, 2024, **64**, e202418348.
22 J. Ochi, Y. Yamasaki, K. Tanaka, Y. Kondo, K. Isayama, S. Oda, M. Kondo and T. Hatakeyama, *Nat. Commun.*, 2024, **15**, 2361.
23 T. Hua, X. Cao, J. Miao, X. Yin, Z. Chen, Z. Huang and C. Yang, *Nat. Photonics*, 2024, **18**, 1161–1169.
24 X. Xiong, T. F. Chen, R. Walia, X. C. Fan, Y. C. Cheng, H. Wang, H. Wu, X. K. Chen, J. Yu, K. Wang and X. H. Zhang, *Angew. Chem., Int. Ed.*, 2025, **64**, e202414882.
25 S. Wu, D. Chen, M. Seinfeld, A. P. McKay, D. B. Cordes, X. Zhang and E. Zysman-Colman, *Chem. Sci.*, 2025, **16**, 15256–15264.
26 M. Nagata, H. Min, E. Watanabe, H. Fukumoto, Y. Mizuhata, N. Tokitoh, T. Agou and T. Yasuda, *Angew. Chem., Int. Ed.*, 2021, **60**, 20280–20285.
27 T. Hua, L. Zhan, N. Li, Z. Huang, X. Cao, Z. Xiao, S. Gong, C. Zhou, C. Zhong and C. Yang, *Chem. Eng. J.*, 2021, **426**, 131169.
28 I. S. Park, H. Min and T. Yasuda, *Angew. Chem., Int. Ed.*, 2022, **61**, e202205684.
29 I. S. Park, M. Yang, H. Shibata, N. Amanokura and T. Yasuda, *Adv. Mater.*, 2022, **34**, 2107951.
30 Y. X. Hu, J. Miao, T. Hua, Z. Huang, Y. Qi, Y. Zou, Y. Qiu, H. Xia, H. Liu, X. Cao and C. Yang, *Nat. Photonics*, 2022, **16**, 803–810.
31 Y. Wang, K. Zhang, F. Chen, X. Wang, Q. Yang, S. Wang, S. Shao and L. Wang, *Chin. J. Chem.*, 2022, **40**, 2671–2677.
32 X. F. Luo, H. X. Ni, A. Q. Lv, X. K. Yao, H. L. Ma and Y. X. Zheng, *Adv. Opt. Mater.*, 2022, **10**, 2200504.
33 S. Cai, G. S. M. Tong, L. Du, G. K. So, F. F. Hung, T. L. Lam, G. Cheng, H. Xiao, X. Chang, Z. X. Xu and C. M. Che, *Angew. Chem., Int. Ed.*, 2022, **61**, e202213392.
34 J. Wang, N. Li, C. Zhong, J. Miao, Z. Huang, M. Yu, Y. X. Hu, S. Luo, Y. Zou, K. Li and C. Yang, *Adv. Mater.*, 2023, **35**, 2208378.
35 Y. Hu, J. Miao, C. Zhong, Y. Zeng, S. Gong, X. Cao, X. Zhou, Y. Gu and C. Yang, *Angew. Chem., Int. Ed.*, 2023, **62**, e202302478.
36 Z. Chen, D. Liu, M. Li, Y. Jiao, Z. Yang, K. Liu and S. J. Su, *Adv. Funct. Mater.*, 2024, **34**, 2404278.
37 J. Jin, S. Wang, H. Jiang, L. Wang and W. Y. Wong, *Adv. Opt. Mater.*, 2024, **12**, 2302354.
38 Y. Zou, M. Yu, Y. Xu, Z. Xiao, X. Song, Y. Hu, Z. Xu, C. Zhong, J. He, X. Cao, K. Li, J. Miao and C. Yang, *Chem*, 2024, **10**, 1485–1501.
39 X. F. Song, S. Luo, N. Li, X. Wan, J. Miao, Y. Zou, K. Li and C. Yang, *Angew. Chem., Int. Ed.*, 2025, **64**, e202413536.
40 Q. Zheng, Y.-K. Qu, P. Zuo, H.-T. Yuan, Y.-J. Yang, Y.-C. Qiu, L.-S. Liao, D.-Y. Zhou and Z.-Q. Jiang, *Chem*, 2025, **11**, 102353.
41 Y. Zhang, D. Zhang, J. Wei, Z. Liu, Y. Lu and L. Duan, *Angew. Chem., Int. Ed.*, 2019, **58**, 16912–16917.
42 Y. Xu, C. Li, Z. Li, Q. Wang, X. Cai, J. Wei and Y. Wang, *Angew. Chem., Int. Ed.*, 2020, **59**, 17442–17446.
43 M. Yang, S. Shikita, H. Min, I. S. Park, H. Shibata, N. Amanokura and T. Yasuda, *Angew. Chem., Int. Ed.*, 2021, **60**, 23142–23147.

44 Y. Liu, X. Xiao, Z. Huang, D. Yang, D. Ma, J. Liu, B. Lei, Z. Bin and J. You, *Angew. Chem., Int. Ed.*, 2022, **61**, e202210210.
45 G. Chen, J. Wang, W. Chen, Y. Gong, N. Zhuang, H. Liang, L. Xing, Y. Liu, S. Ji, H. Zhang, Z. Zhao, Y. Huo and B. Z. Tang, *Adv. Funct. Mater.*, 2023, **33**, 2211893.
46 Z. Huang, H. Xie, J. Miao, Y. Wei, Y. Zou, T. Hua, X. Cao and C. Yang, *J. Am. Chem. Soc.*, 2023, **145**, 12550–12560.
47 S. Luo, J. Wang, N. Li, X. F. Song, X. Wan, K. Li and C. Yang, *Angew. Chem., Int. Ed.*, 2023, **62**, e202310943.
48 X. Song, S. Shen, S. Zou, Y. Wang, F. Guo, S. Gao and Y. Zhang, *Chem. Eng. J.*, 2024, **481**, 148794.
49 X. Xiong, J. Q. Li, T. F. Chen, X. C. Fan, Y. C. Cheng, H. Wang, F. Huang, H. Wu, J. Yu, X. K. Chen, K. Wang and X. H. Zhang, *Adv. Funct. Mater.*, 2024, **34**, 2313726.
50 J. M. Jin, D. Liu, W. C. Chen, C. Shi, G. Chen, X. Wang, L. Xing, W. Ying, S. Ji, Y. Huo and S. J. Su, *Angew. Chem., Int. Ed.*, 2024, **63**, e202401120.
51 L. Xing, J. Wang, W. C. Chen, B. Liu, G. Chen, X. Wang, J. H. Tan, S. S. Chen, J. X. Chen, S. Ji, Z. Zhao, M. C. Tang and Y. Huo, *Nat. Commun.*, 2024, **15**, 6175.
52 D. Chen, H. Wang, D. Sun, S. Wu, K. Wang, X. H. Zhang and E. Zysman-Colman, *Adv. Mater.*, 2024, **36**, 2412761.
53 J. Jin, Z. He, D. Liu, Y. Mei, J. Wang, H. Wan and J. Li, *Chem. Sci.*, 2024, **15**, 18135–18145.
54 S. Li, Z. Yang, Y. Xie, L. Hua, S. Ying, Y. Liu, Z. Ren and S. Yan, *Chem. Sci.*, 2024, **15**, 18335–18346.
55 F. Liu, Z. Cheng, W. Dong, Y. Yan, Y. Xu, Z. Su, Y. Hu, L. Wan and P. Lu, *Angew. Chem., Int. Ed.*, 2025, **64**, e202416154.
56 R. Z. An, F. M. Zhao, C. Shang, M. Zhou and L. Cui, *Angew. Chem., Int. Ed.*, 2025, **64**, e202420489.
57 X. Wu, B.-K. Su, D.-G. Chen, D. Liu, C.-C. Wu, Z.-X. Huang, T.-C. Lin, C.-H. Wu, M. Zhu, E. Y. Li, W.-Y. Hung, W. Zhu and P.-T. Chou, *Nat. Photonics*, 2021, **15**, 780–786.
58 J. H. Williams, *Acc. Chem. Res.*, 1993, **26**, 593–598.
59 M. A. El-Sayed, *J. Chem. Phys.*, 1963, **38**, 2834–2838.
60 M. Einzinger, T. Zhu, P. de Silva, C. Belger, T. M. Swager, T. Van Voorhis and M. A. Baldo, *Adv. Mater.*, 2017, **29**, 1701987.
61 F. Wang, J. Ye, J. Liu, X.-K. Chen, Y. Yang, Z. Bin and J. You, *Angew. Chem., Int. Ed.*, 2025, **64**, e202502380.
62 Y. Song, K. Zhang, P. Wang, Y. Cao and L. He, *Adv. Funct. Mater.*, 2025, **35**, 2411957.
63 S. Xu, Q. Yang, Y. Zhang, H. Li, Q. Xue, G. Xie, M. Gu, J. Jin, L. Huang and R. Chen, *Chin. Chem. Lett.*, 2021, **32**, 1372–1376.
64 Y. Qi, W. Ning, Y. Zou, X. Cao, S. Gong and C. Yang, *Adv. Funct. Mater.*, 2021, **31**, 2102017.
65 M. Colella, A. Danos and A. P. Monkman, *J. Phys. Chem. Lett.*, 2019, **10**, 793–798.
66 K. Goushi, K. Yoshida, K. Sato and C. Adachi, *Nat. Photonics*, 2012, **6**, 253–258.
67 Y. Song, K. Zhang, Y. Li, Y. Shu, Y. Xiu and L. He, *Adv. Funct. Mater.*, 2025, **35**, 2422927.
68 (*a*) CCDC 2435331: Experimental Crystal Structure, 2025, DOI: **10.5517/ccdc.csd.cc2mr52n**; (*b*) CCDC 2435332: Experimental Crystal Structure, 2025, DOI: **10.5517/ccdc.csd.cc2mr53p**; (*c*) CCDC 2435333: Experimental Crystal Structure, 2025, DOI: **10.5517/ccdc.csd.cc2mr54q**; (*d*) CCDC 2435337: Experimental Crystal Structure, 2025, DOI: **10.5517/ccdc.csd.cc2mr58v**.